Ocean Sci. Discuss., 7, 1469–1495, 2010
www.ocean-sci-discuss.net/7/1469/2010/
doi:10.5194/osd-7-1469-2010

Ocean Science Discussions

The influence of temperature and salinity variability on the upper ocean density and mixed layer

R. W. Helber, J. G. Richman, and C. N. Barron

Naval Research Laboratory, Ocean Dynamics and Prediction Branch – Code 7321, Stennis Space Center, MS 39529, USA

Received: 4 August 2010 – Accepted: 6 August 2010 – Published: 17 August 2010

Correspondence to: R. W. Helber (robert.helber@nrlssc.navy.mil)

Published by Copernicus Publications on behalf of the European Geosciences Union.

Abstract

The relative influence of both temperature and salinity on the mixed layer depth (MLD) is evaluated using a relationship of binned regressions of MLD on vertical density compensation and isothermal layer depth (ILD) from a global set of in situ profile observations. Our approach is inspired by the observations of the difference between the MLD and the sonic layer depth (SLD) that evolve seasonally around the global ocean. In this article, we hypothesize that vertical density compensation governs SLD-MLD differences and can be used for mapping the relative influence of temperature and salinity on upper ocean structure. The Turner angle, computed between the surface and 200 m (bulk Turner angle, BTA), serves as a measure of vertical density compensation that quantifies times and areas where either temperature or salinity is destabilizing. For temperature destabilization the ocean exhibits cool/fresh overlying hot/salty water. For salinity destabilization the ocean exhibits hot/salty overlying cool/fresh water. These two classes of density compensation have seasonal variability with different geographical characteristics. Profiles with salinity controlled stable density and destabilizing temperature gradient are found most often at high latitudes. Profiles with temperature controlled stable density and destabilizing salinity gradient are found in the tropics and subtropics of all oceans. Results indicate that about half of the ocean has vertical density compensation that is a necessary condition for SLD-MLD differences. While density compensation is necessary, it is not a sufficient condition for predicting the dependence of MLD on BTA. Density compensation is the dominant factor in MLD variability in heavy river input and subduction regions that cover only ∼14% of the ocean.

1 Introduction

The upper ocean typically is characterized by a surface boundary layer with nearly uniform temperature and salinity, and this layer may also act as acoustic duct to trap sound near the surface. The thickness of the uniform layer and the acoustic duct

OSD
7, 1469–1495, 2010

are determined by the location of a strong gradient in the density and sound speed, respectively. Two measures of the thickness of this layer, the mixed layer depth (MLD) and sonic layer depth (SLD) are often the same, but significant differences between the MLD and SLD do occur (Helber et al., 2008). An explanation for the SLD-MLD differences and the broader implications of this finding, however, are incomplete. The present article explores the underlying temperature and salinity structures that lead to SLD-MLD differences while providing a global view of the competing influences of temperature and salinity useful for broad application to oceanographic investigation of the upper ocean structure and variability.

Temperature and salinity influence the density and sound speed in different ways. Sound speed increases with temperature and salinity, although the relative influence of salinity is weak, as indicated by the nearly vertical isotachs in Fig. 1a. In contrast, density increases with salinity but decreases with temperature. Since salinity has a stronger influence on density than on sound speed, the slope of the iso-lines in Fig. 1b are not as steep as those in Fig. 1a. The opposite slopes of the iso-lines in Fig. 1a, b indicate that density and sound speed depend on temperature in opposite directions while they depend on salinity in the same direction. Given this relationship, we hypothesize that the vertical density compensation governed by the relative contributions of temperature and salinity in the upper ocean controls where SLD-MLD differences occur.

As a measure of the vertical density compensation in the upper ocean, we use the Turner angle, *Tu* (Ruddick, 1983). The Turner angle is closely related to the well known density gradient ratio, R_ρ (Turner, 1973), and was originally used as a measure of double-diffusive ocean conditions. We compute the Turner angle from temperature and salinity differences between the near surface and 200 m depth and hereafter refer to this as the bulk Turner angle (BTA). Since the BTA is a measure over the upper 200 m of the ocean, it is not an indicator of fine-scale double-diffusive processes that typically occur on scales much smaller than 1 m. Instead, it is representative of the broader temperature and salinity structure of the upper ocean. The BTA associated

OSD
7, 1469–1495, 2010

with a destabilizing salinity gradient has been connected to spice injections in the subtropics that lead to interannual isopycnal variations in the ocean interior (Yeager and Large, 2007). The dominant processes for spice injections are wintertime penetrative convection, not double-diffusion.

The observations supporting this study are a comprehensive collection of ocean profiles of temperature and salinity extending from the early 1960's to the present, including the Argo profiling float data set. For each quality controlled profile, SLD, MLD, and BTA values are computed. Using conditional probabilities, we demonstrate that SLD-MLD differences tend to occur for profiles where the BTA values identify vertical density compensation.

SLD-MLD differences, however, have limited applicability for describing dynamic characteristics of the upper ocean. SLD, for example, is a measure of the depth of an acoustic surface duct and not directly linked to ocean dynamics. A clear connection emerges when regressions of temperature and salinity structure on MLD are used to construct a density compensation index. This index identifies regions of the ocean where vertical density compensation controls mixed layer variability. Thus, using the basic properties of temperature and salinity in the upper ocean, we highlight conditions where temperature and salinity compete for control and the dynamic and acoustic variability are fundamentally different.

The global set of temperature and salinity profile pairs comes from three major data centers and is described in Sect. 2. Although the spatial and temporal data collectively spans the mesoscale, the observations generally are not coherent. Each individual profile is nearly instantaneous providing a snapshot of the vertical structure of finer scale variability. As a result, a statistical measure of prevalent features begins to emerge from the numerous profiles taken randomly in space and time. Section 3 contains descriptions of the BTA, MLD, and SLD, Sect. 4 presents the conditional probabilities which establish that density compensation in the vertical is required for significant differences in the MLD and SLD, and Sect. 5 describes the geographical variability and regime characteristics. A compensation index, which highlights the role of density

OSD
7, 1469–1495, 2010

compensation in determining the mixed layer variability, is described in Sect. 6 with summary and conclusions in Sect. 7.

2 Profile observations

In situ profile observation pairs of temperature and salinity are taken from the Navy's Master Oceanographic Observation Data Set (MOODS) (Teague et al., 1990), the National Ocean Data Center's World Ocean Dataset 2005 (WOD05) (Boyer et al., 2006), and the global ocean profiling float array, Argo (Roemmich et al., 2004). The data sources for MOODS and WOD05 extend from some of the first reliable ocean temperature and salinity observations in the early 20th century and through 2005 for WOD05 and 2007 for MOODS. Duplicates are removed as these data sets substantially overlap, but each contributes unique profiles. The Argo data in this analysis range from 1995 through 2007. The Argo profiles recorded in the MOODS and WOD05 sets are superseded by data obtained directly from the Argo data acquisition centers, as the latter records may have undergone additional quality control procedures designed specifically for profiling floats.

The complete initial data set contains 2 118 299 profiles with paired temperature and salinity. To be used in our analysis, a profile must meet a set of minimum standards. Each profile must have (1) no non-standard quality control flags as provided by MOODS, WOD05 or Argo, (2) the shallowest depth sample no deeper than 10 m, (3) its maximum interval between depth samples less than 25 m in the upper 150 m, 50 m in the depth range from 150 m to 300 m, and 100 m below 300 m, and (4) the total depth coverage of the profile at least 200 m. After these editing steps the resulting subset retains 453 213 profiles.

OSD
7, 1469–1495, 2010

T/S compensation on upper ocean structure

R. W. Helber et al.

3 Metrics

3.1 The bulk Turner angle

The Turner angle is used in turbulence research to identify regimes of double-diffusive processes. The computation is related to the vertical density gradient ratio, R_ρ, which is defined as the ratio of the change in density due to temperature over the change in density due to salinity, or

$$R_\rho = \frac{\alpha \partial_z T}{\beta \partial_z S}, \tag{1}$$

where α and β are the expansion coefficients for temperature (T) and salinity (S), respectively. The value of R_ρ becomes infinite when $\beta \partial_z S$ approaches zero, leading Ruddick (1983) to introduce the Turner angle, *Tu*. Following Yeager and Large (2007), *Tu* is given by:

$$Tu = \tan^{-1}\left(\frac{\alpha \partial_z T + \beta \partial_z S}{\alpha \partial_z T - \beta \partial_z S}\right) = \tan^{-1}\left(\frac{R_\rho + 1}{R_\rho - 1}\right). \tag{2}$$

The Turner angle is discussed in the recent literature (e.g., Johnson, 2006), has been applied to both horizontal (Tippins and Tomczak, 2003) and vertical gradients (Yeager and Large, 2007), and has been computed globally from climatology (You, 2002).

In our analysis, the Turner angle is computed for vertical finite differences of T and S over a depth range of ∼200 m. From each profile pair of T and S, the differences,

$$\partial_z T \cong \frac{\Delta T}{\Delta z} = \frac{T(z_0) - T(z_0 + 200)}{200} \tag{3}$$

and

$$\partial_z S \cong \frac{\Delta S}{\Delta z} = \frac{S(z_0) - S(z_0 + 200)}{200}, \tag{4}$$

OSD
7, 1469–1495, 2010

are computed between a reference depth, z_0, and 200 m below that depth. We have defined the reference depth (z_0) in this analysis to be 8 m. For profiles that have T and S values at or above 8 m, the values for $T(z_0)$ and $S(z_0)$ are obtained by linear interpolation between surrounding values of the observation profile. The values for $T(z_0+200)$ and $S(z_0+200)$ are also obtained by linear interpolation between surrounding values to 208 m depth. Profiles that have no value at or above 8 m or at or below 208 m are not used. The reference of z_0=8 m allows the use of Argo profiles that start near 5 m and avoids much of the potential influence of the shallow diurnal warming. Given the possible depth sampling following the profile selection described in Sect. 2, the deep observation values could be as large as 25 m from the target depth, but deviations that large are not likely. The Tu computed by this technique is termed the bulk Turner angle (BTA).

The BTA can have a value between −180° to 180°. For values with greater magnitude than 90°, either positive or negative, the upper ocean water column is statically unstable. Unstable profiles fall in the lower right non-shaded part of Fig. 2. In the present analysis, unstable profiles are discarded. For Tu values between −45° and 45°, the profiles are doubly stable, with both temperature and salinity contributing to a stable density. The Turner angles −45° and 45° (bounding the upper left quadrant) identify conditions where the vertical gradients of temperature (−45°) or salinity (45°) are zero and thus do not contribute to the density gradient. The corresponding density ratio equals zero for BTA=−45° and infinity for BTA=45°. BTA values between 45° and 90° represent the salinity destabilizing (hot/salty over cool/fresh or salt-fingering at small scales) regime, while BTA values between −90° and −45° represent the temperature destabilizing (cool/fresh over hot/salty or diffusive at small scales) regime.

We can use the BTA to determine the degree of density compensation provided by the individual temperature and salinity gradients. In Fig. 2, density compensation occurs in the upper right and lower left quadrants. In the temperature destabilizing regime (lower left quadrant), a temperature inversion (cold over hot) reduces the overall stability provided by the stabilizing salinity gradient (fresh over salty). Conversely, in

OSD
7, 1469–1495, 2010

the salinity destabilizing regime (upper right quadrant), a salinity inversion (salty over fresh) reduces the overall stability provided by the stabilizing temperature gradient (hot over cold). It is important to realize that taking the difference over 200 m changes the nature of the BTA computation from the original fine scale interpretation for *Tu*. Double diffusive processes (fingering or diffusive) typically are associated with small scale turbulence, and compensating values of the BTA do not necessarily suggest that double diffusion is a dominant process over the 200 m depth range.

3.2 Mixed and sonic layer depths

The mixed layer depth typically is estimated by either a threshold method (e.g., Kara et al., 2000; de Boyer Montégut et al., 2004), or a curvature method (Bathen, 1972; Belkin and Flyushkin, 1986; Lorbacher et al., 2006) using either the temperature or potential density profile. Threshold methods are the easiest to implement for automatic detection of the MLD. However, careful inspection of the observations shows that the optimal choice of the threshold value changes regionally and seasonally (Kara et al. 2003). Early curvature methods to estimate the MLD were difficult to implement for automatic detection and not particularly robust. The present analysis uses a robust freely available curvature method from Lorbacher et al. (2006).

The SLD represents the thickness of the surface acoustic duct, a layer where sound is trapped near the surface by upward refraction due to increasing sound speed with depth (Helber et al., 2008). The key characteristic of both MLD and SLD is that both represent the depth at which the structure of the upper ocean sharply changes. MLD identifies the depth where density sharply changes whereas SLD identifies the depth where sound speed sharply changes. SLD and MLD differ when ocean temperature and salinity compete for control of either density or sound speed gradients.

For most of the ocean, MLD and SLD do not differ significantly. Typically an isothermal/isohaline surface layer exists and both MLD and SLD are located at the base of this layer. Below the MLD/SLD a significant difference between the sound speed and density occurs, with density increasing while sound speed typically decreases. For most

OSD
7, 1469–1495, 2010

profiles, temperature dominates the upper ocean structure, and decreasing temperature below the MLD/SLD leads to increasing density and decreasing sound speed. In specific seasons and geographic regions of the ocean, however, salinity plays a more important role in the density and sound speed structure. When temperature and salinity become competing factors, values of MLD and SLD can diverge.

4 Conditional probabilities

The differences in the sensitivities of density and sound speed to T and S will be exploited by comparing the BTA with the layer depth difference, SLD minus MLD. We hypothesize that for certain density ratios, the differences in sensitivities of density and sound speed to T and S will lead to differences between SLD and MLD.

To understand the connection between the BTA and SLD-MLD, we construct conditional seasonal probability distributions globally from all available observation profiles. We bin the data to treat the Northern and Southern Hemisphere seasons in phase. Early-spring represents Northern Hemisphere months of January, February, and March and the Southern Hemisphere months of July, August, and September. Similarly, early-fall represents Northern Hemisphere months of July, August, and September and the Southern Hemisphere months of January, February, and March. Standard conditional probability (e.g., Wilks, 2006) is computed using 10° bins for BTA and 20 m bins for SLD-MLD differences. These bins are represented by the colored trapezoids of the polar plots in Fig. 3.

The polar plots depict probability distributions with stable BTA values of $-90° \leq \text{BTA} \leq 90°$ and SLD-MLD difference values of $0\,\text{m} \leq \text{SLD-MLD} \leq 310\,\text{m}$ for the upper left hemisphere and $0\,\text{m} \geq \text{SLD-MLD} \geq -70\,\text{m}$ for the lower right hemisphere. Figure 3a, b shows the probability that a profile with a given SLD-MLD also has a BTA within a 10° range. Probabilities along an arc of a given radius sum to one. Conversely, Fig. 3c, d shows the probability that a profile with a given BTA also has a SLD-MLD difference within a 20 m range. Probabilities along a radial at a given angle sum to one.

OSD
7, 1469–1495, 2010
T/S compensation on upper ocean structure
R. W. Helber et al.

Figure 3a,c are for early-spring and Fig. 3 b,d are for early fall.

In Fig. 3a, we see relatively high probabilities occur for large SLD-MLD differences in the temperature destabilizing regime with BTA values between −45° and −75° in early-spring. For example, given a SLD-MLD difference between 210 and 230 m, there is approximately a 30% chance of a BTA between −50° and −60°. Another relatively high probability early-spring regime occurs for SLD-MLD differences between 50 and 150 m for BTA values in the salinity destabilizing regime between 45°and 75°. Given a SLD-MLD difference between 90 and 110 m, there is approximately a 15% chance of a BTA between 60° and 70°. Even in these relatively high probability regions, the actual probabilities are small, <0.3 (or 30%). As noted by Helber et al. (2008), large SLD-MLD differences in general are a relatively infrequent occurrence.

During early-fall, the conditional probabilities are substantially different (Fig. 3b). Given large SLD-MLD differences, high probabilities generally only occur when temperature stratification is very weak, resulting in BTA values near −45°. The large differences occur because the MLD algorithm is unable to identify a clear mixed layer when temperature stratification is very weak, resulting in a wide variance of values that differ from the SLD. While these cases identify a failure of the MLD algorithm, they characterize the nature of the upper ocean temperature and salinity structure. Relatively large probabilities also occur for BTA values near 45°. The substantial lack of large SLD-MLD differences in early-fall, for BTA values other than 45° and −45°, suggests that seasonal deep mixing erases temperature or salinity destabilizing regimes over the upper 200 m. In general, during early-fall the surface ocean is doubly stable with respect to the ocean at 208 m depth (Fig. 3d).

A different look at the relationship between the BTA and SLD-MLD differences can be obtained from the conditional probability of the SLD-MLD difference for a given BTA (Fig. 3c, d). For doubly stable BTA (|BTA|<45°), the SLD-MLD difference is small for virtually all profiles throughout the year. In the salinity destabilizing regime (BTA>45°), approximately 30% of the profiles have small SLD-MLD differences in the spring and nearly all of the profiles have small SLD-MLD differences in the fall. From the conditional probability analysis we find an important result. A destabilizing BTA doesn't always indicate a large difference between the SLD and MLD. However, a large difference between the SLD and MLD always corresponds to a destabilizing BTA.

5 Global variability

5.1 Bulk Turner angle

To investigate seasonal density compensation variability, the BTA values from individual observation profiles are binned by month and into one degree radius circular regions centered on integer latitude and longitude points. Figure 4 shows median BTA values of the bins for March and September. The color scale in Fig. 4 is chosen to highlight the different regimes with the temperature destabilizing profiles colored blue, salinity destabilizing profiles colored red, doubly stable profiles colored yellow and green, and profiles near the transition between stabilizing and destabilizing temperature and salinity ($|BTA| \approx 45^\circ$) colored grey and black. The data coverage is not uniform, as many grid points have no data. Similar figures using Argo profiles are presented in Yeager and Large (2007).

In the tropics and subtropics, the density gradient stability is temperature dominated with BTA>0 (yellow, black, and red colors in Fig. 4), while the higher latitudes are salinity dominated stability with BTA<0 (green, grey, and blue colors in Fig. 4). Generally at high latitudes, the temperature is nearly uniform and the salinity increases with depth. The temperature destabilizing regime with $-90^\circ < BTA < -45^\circ$, has its greatest geographical extent in the Northern (Southern) Hemisphere high-latitudes during March (September). The subpolar gyres of the Northern Hemisphere are temperature destabilized in the winter and spring, but shift to doubly stable in the summer and fall. The Salinity destabilizing regime covers nearly the entire Atlantic ocean and much of the subtropical gyres in the Pacific. The black regions mark the transition between doubly stable and salinity destabilizing regimes and occur along the equator and surrounding the subtropical gyres in the autumn hemisphere.

OSD
7, 1469–1495, 2010
T/S compensation on upper ocean structure
R. W. Helber et al.

A significant fraction of observed profiles show destabilizing tendencies from temperature or salinity. Globally, 49% of all data filled regions in Fig. 4 have a BTA magnitude greater than 45° (|BTA|>45°) with 40% salinity destabilizing (BTA>45°) and 8% temperature destabilizing (BTA<−45°). In the Northern Hemisphere (10° to 60° N) early-spring (January–March), 57% of regions have |BTA|>45° while in the early-fall (July–September) only 47% of the regions have a destabilizing BTA. The seasonality is most pronounced for the temperature destabilizing case since 11% of the regions have BTA<−45° in the Northern Hemisphere in early-spring with only 5% occurring in early-fall.

The present results are consistent with an earlier study by You (2002) who calculated the Turner angle on a 1° by 1° grid from the Levitus (1982) climatology. You found that 44% of the Turner angles have a magnitude greater than 45°, and about 14% of the grid has *Tu*<−45°. The diffusive (or temperature destabilizing) regime tends to be found in the polar and subpolar regions, where surface cooling, excess precipitation and ice melt set the characteristics of the upper ocean. About 30% of You's grid has *Tu*>45°, consistent with the salt fingering or salinity destabilizing limit found in the tropics and subtropics equatorward of 45° latitude, where excess evaporation over precipitation dominates the upper ocean.

5.2 Regime characteristics

We identify two regimes that fall into geographic regions and are defined by the early-spring conditional probability for limited SLD-MLD and BTA ranges (Fig. 3a). The temperature destabilizing (TD) regime is defined by the ranges, −80<BTA<−50 and 150<SLD-MLD<300 while the salinity destabilizing (SD) regime is defined by the ranges, 50<BTA<80 and 50<SLD-MLD<200. Both regimes have relatively large percentages of occurrence and exist in different geographical regions and opposite BTA ranges. In each regime, the profiles tend to have distinctive shapes and characteristics.

The temperature destabilizing (TD) regime has relatively large SLD-MLD differences associated with cold-fresh water over warm-salty water. A typical profile from the

OSD
7, 1469–1495, 2010

subpolar North Atlantic, with very cold water near the surface with warmer saltier water below, can be seen in the example shown in Fig. 5. Most of the TD profiles are found at high latitudes in the winter hemisphere.

The salinity destabilizing (SD) regime has a globally wide spread occurrence in the tropics and subtropics. The SLD-MLD differences here are not as large as those in the TD regime. We see in the example profile (Fig. 6) a relatively deep, nearly isothermal upper layer (or deep isothermal layer depth, ILD), but a near surface temperature increase makes the MLD much shallower than the SLD. The deep ILD is characteristic of mode waters originating at the outcroppings of density layers or thermocline ventilation (e.g., Johnson, 2006; Wong and Johnson, 2003; Hanawa and Talley, 2001). Such waters are thought to carry the spice injections described by Yeager and Large (2007). The mode water properties are set by the local processes that alter the buoyancy of the mixed layer, but details about how subduction occurs are not well understood. In the simulations of Yeager and Large (2007) a strongly density compensated layer forms below the mixed layer in the early-spring, which decouples the mixed layer T and S characteristics from the subducted mode water. Because the mixed layer is decoupled from the subducted mode water, the ILD may be more representative of the SLD than the MLD.

6 Compensation index

From the maps of the BTA, we find that most of the subtropical oceans fall in the salinity destabilizing regime and much of the subpolar oceans fall in the temperature destabilizing regimes. From the conditional probabilities discussed in Sect. 4, however, we find for a given BTA range less than approximately 30% of all profiles also have large SLD-MLD differences. Thus, while the temperature or salinity destabilizing regimes are necessary for large SLD-MLD differences, they are not sufficient. Other conditions must also be present for SLD-MLD differences to occur. To further isolate the unique conditions required for SLD-MLD differences, we derive a method for determining where the density compensated stratification is most influential on the upper ocean structure.

OSD

7, 1469–1495, 2010

Focusing on the influence of temperature versus salinity, we will use the isothermal layer depth (ILD) instead of the SLD in this section. The SLD has a strong dependence on pressure which helps to magnify SLD-MLD differences in destabilizing regimes but adds an additional variable we now wish to eliminate. In addition, ILD is computed in the same way as MLD but using only temperature profiles rather than density. ILD is a temperature only version of MLD that also acts as a proxy for SLD since SLD is more strongly influenced by temperature than salinity relative density.

Consider three linear regression models to empirically predict MLD from BTA and ILD. The regression equations are:

$$\mathrm{MLD_{BI}} = a_{\mathrm{BI}}\mathrm{BTA} + b_{\mathrm{BI}}\mathrm{ILD} + c_{\mathrm{BI}} \quad (5)$$

$$\mathrm{MLD_{B}} = a_{\mathrm{B}}\mathrm{BTA} + c_{\mathrm{B}} \quad (6)$$

$$\mathrm{MLD_{I}} = b_{\mathrm{I}}\mathrm{ILD} + c_{\mathrm{I}} \quad (7)$$

In Eqs. (5)–(7), the constants a, b, and c are determined from least square regression. The subscripts in Eq. (5), BI, indicate the both BTA and ILD are used as the regressors. In Eqs. (6) and (7), BTA and ILD are the sole regressors with B and I as the subscripts, respectively. Each regression has a goodness of fit r^2 value, r^2_{BI}, r^2_{B}, and r^2_{I} where a perfect linear fit would have an r^2 at its maximum of value of one.

Equation (5) has the most information and flexibility to form an empirical prediction of MLD and returns the largest goodness-of-fit value, r^2_{BI}. The regressions in Eqs. (6) and (7) are less skillful depending on the density compensation, and the goodness-of-fit values, r^2_{B} and r^2_{I}, tend to be smaller than r^2_{BI}.

The compensation index is constructed from r^2_{BI}, r^2_{B}, and r^2_{I} and is given by

$$\mathrm{CI} = 2\frac{r^2_{\mathrm{B}}}{r^2_{\mathrm{BI}}} + \frac{r^2_{\mathrm{I}}}{r^2_{\mathrm{BI}}} - 1\,.$$

The compensation index equals one when the MLD regression is entirely controlled by BTA with no influence by the ILD, meaning the goodness of fit r^2_{B} equals r^2_{BI} and r^2_{I}=0. In

OSD
7, 1469–1495, 2010

those areas, salinity variations dominate. If instead, the regression is controlled entirely by ILD (r_B^2=0 and r_I^2=r_{BI}^2), the compensation index is equal to zero and temperature is the sole contributor to variations in MLD.

In Fig. 7, the compensation index tends to be near 1 at high latitudes, where temperature destabilizing condition occur with cold/fresh overlying hot/salty water, and also at mid-latitudes, where salinity destabilizing conditions occur with hot/salty overlying cold/fresh water. The salinity destabilizing BTA dominates the subtropics of the Atlantic and Pacific Oceans and the Arabian Sea, but the compensation index is large particularly in the eastern subtropics of the Atlantic and South Pacific, where subduction occurs. Regions influenced by large river input, such as the Amazon and Ganges, have larger compensation index values than the surrounding ocean.

By comparing Figs. 7 and 4, we find that the compensation index is near one in most of the temperature destabilizing regions located at high latitudes and substantially fewer of the salinity destabilizing regions of the subtropics. In both destabilizing regimes, large compensation index tends to be in a subset of all areas of large vertical density compensation. While part of the discrepancy may be due to the compensation index representing all seasons while Fig. 4 show only two seasons, it is consistent with the conditional probabilities in Sect. 4 that indicate large SLD-MLD differences occur in less that 30% of all destabilizing regimes. In addition, it is consistent that compensation index is large precisely in known subduction regions of the South Pacific and Atlantic and the North Atlantic subtropics.

7 Summary and conclusions

The upper ocean is characterized by a layer of nearly uniform temperature and salinity with a sharp gradient below this layer. The depth of this layer may be determined from the temperature as the isothermal layer depth (ILD), from density as the mixed layer depth (MLD) and from sound speed as the sonic layer depth (SLD). These three measures have differences that evolve seasonally and regionally around the global

OSD
7, 1469–1495, 2010

ocean. The present paper focuses on explaining the observed SLD-MLD differences while highlighting the competing influences of temperature and salinity on the vertical structure of the global ocean density field. The observations consist of a comprehensive collection of in situ ocean profiles of temperature and salinity from three different ocean data centers. Using the bulk Turner angle (BTA) computed from temperature and salinity changes from the surface to 200 m, we show through conditional probabilities that large SLD-MLD differences are found only when vertical density compensation occurs. Thus, density compensation is required for large SLD-MLD differences,but not every compensated profile has a large SLD-MLD difference.

While SLD-MLD differences highlight regions of the ocean where temperature and salinity compete for control of the upper ocean, SLD is primarily an acoustic metric and is not directly related to ocean circulation. The SLD, in addition, includes the influence of pressure on sound speed. To provide a similar measure of the competing influence of temperature and salinity in the upper ocean, without the influence of pressure, we replace the SLD with the isothermal layer depth (ILD). The ILD uses the temperature only and represents the upper ocean characteristics when temperature dominates. Using the ILD, we formulate a compensation index that allows us to identify regions of the ocean where vertical density compensation impacts the mixed layer. Results show that the BTA has superior "goodness of fit" with MLD in subduction regions of the subtropics of the North and South Atlantic and South Pacific and in regions of large river input such as in the Bay of Bengal and the Equatorial Atlantic near the Amazon River outflow. MLD is also predicted well by BTA in a large region of the North Pacific. In all of these areas, the competing influence of temperature and salinity or density compensation has a large influence on the MLD.

For the global ocean, 51% of the 4° by 4° regions have doubly stable BTA values and 48% of the regions have compensation index less than 0.2. Thus, about half of the ocean is either doubly stable or temperature dominated. For the remaining 49% of the ocean where either temperature or salinity is destabilizing, temperature and salinity compete for control of the upper ocean structure. In early-spring, temperature

OSD
7, 1469–1495, 2010

destabilization occurs at high latitudes and salinity destabilization occurs at mid latitudes. Density compensation is the dominant factor in MLD variability in 14% of regions where the compensation index is greater than 0.8, indicating that temperature and salinity compete for control of the MLD variability. For data binned by 20 m increments of SLD-MLD differences, less than 30% of profiles are temperature destabilizing and less than 20% are salinity destabilizing. Since SLD includes the influence of pressure, SLD-MLD differences provide a related but different view of the competing influence of temperature and salinity.

Large SLD-MLD differences occur more often at high latitudes during early-spring when cold/fresh overlies hot/salty water. More specifically, for a SLD-MLD difference of 210–230 m in the early spring, the BTA is likely to be in the temperature destabilizing regime in more than 50% of all profiles (obtained by summing the temperature destabilizing conditional probabilities in the 210–230 m SLD-MLD range in Fig. 3a). Conversely, smaller SLD-MLD differences occur more often at mid-latitudes in sub-tropical gyres when hot/salty overlies cold/fresh water. For a SLD-MLD difference of 70–90 m in the early spring, the BTA is likely to be defined by the salinity destabilizing regime in nearly 40% of all profiles (obtained by summing the salinity destabilizing conditional probabilities in the 70–90 m SLD-MLD range in Fig. 3a).

In general, large differences in SLD-MLD are relatively infrequent. This can be seen for conditional probabilities given a BTA range. For BTA values between -50° to -80°, there is only 15% probability of finding SLD-MLD differences in the range of 210–230 m (obtained by summing the conditional probabilities from -50° to -90° BTA in the 210–230 m SLD-MLD range in Fig. 3c).

This work provides a fundamental description of the upper ocean by mapping the regions of the ocean where vertical density compensation is an important factor in the evolution of the upper ocean structure. The dynamical and acoustical properties of the ocean behave differently in vertically compensated regions of the ocean. Salinity has traditionally been poorly observed and modeled, but the recent availability of Argo salinity and improvements in satellite precipitation observations enable more accurate study of salinity variability.

Knowledge of when and where the MLD and SLD differ significantly and where the compensation index is near one can have important implications for a variety of applications from Navy operations concerned with ocean acoustics to climate related air-sea interactions. Our analysis shows that density compensation as indicated by temperature or salinity destabilizing gradients is required to have large differences in the acoustic, thermal and density structure of the upper ocean. For salinity destabilizing regimes, the large differences also occur in regions of subduction and mode water formation. The mechanisms which establish these destabilizing gradients are not clear. Horizontally towed observations (Rudnick and Martin, 2002) in these regions show density compensation within the mixed layer, which may be important for the export of temperature-salinity variability, or spice, into the ocean interior. Having a statistical representation of the density compensation characteristics of the upper ocean could be used to infer expected behavior of the sub-mesoscale variability, which responds differently to compensated versus non-compensated fronts. These effects may be important particularly for improving the next generation of sub-mesoscale resolving operational ocean prediction systems.

Acknowledgements. This publication is a contribution to the Improved Synthetic Ocean Profile (ISOP) project supported by the Office of Naval Research under program element 602345N. The authors greatly appreciate the skillful rendering of Fig. 2 by Jan Dastugue. This is contribution NRL/JA/7320—10-0416 and has been approved for public release.

References

Bathen, K. H.: On the seasonal changes in the depth of the mixed layer in the North Pacific Ocean, J. Geophys. Res., 77, 7138–7150, 1972.

Belkin, I. M. and Filyushkin, B. N.: Seasonal variability of upper ocean thermal structure in the POLYMODE study area, Oceanology, 26, 149–154, 1986.

de Boyer Montégut, C., Madec, G., Fischer, A. S., Lazar, A., and Iudicone, D.: Mixed layer depth over the global ocean: an examination of profile data and a pofile-based climatology, J. Geophys. Res., 109, C12003, doi:10.1029/2004JC002378, 2004.

Boyer, T. P., Antonov, J. I., Garcia, H. E., Johnson, D. R., Locarnini, R. A., Mishonov, A. V., Pitcher, M. T., Baranova, O. K., and Smolyar, I. V.: Introduction, in: World Ocean Database 2005, edited by: Levitus, S., NOAA Atlas NESDIS 60, US Government Printing Office, Washington, DC/USA, 190 pp., 2006.

Hanawa, K. and Talley, L. D.: Mode waters, in: Ocean Circulation and Climate – Observing and Modeling the Global Ocean, edited by: Siedler, G., Church, J., and Gould, J., Academic Press, San Diego, CA, 373–386, 2001.

Helber, R. W., Barron, C. N., Carnes, M. R., and Zingarelli, R. A.: Evaluating the sonic layer depth relative to the mixed layer depth, J. Geophys. Res., 113, C07033, doi:10.1029/2007JC004595, 2008.

Johnson, G. C.: Generation and initial evolution of a mode water θ–s anomaly, J. Phys. Oceanogr., 36, 739–751, 2006.

Kara, A. B., Rochford, P. A., and Hurlburt, H. E.: An optimal definition for ocean mixed layer depth, J. Geophys. Res., 105, 16803–16821, 2000.

Kara, A. B., Rochford, P. A., and Hurlburt, H. E.: Mixed layer depth variability over the global ocean, J. Geophys. Res., 108, 3079, doi:10.1029/2000JC000736, 2003.

Levitus, S.: Climatological atlas of the world ocean, Professional paper 13, NODC Ocean Climate Laboratory, Washington, DC, 1982.

Lorbacher, K., Dommenget, D., Niiler, P. P., and Köhl, A.: Ocean mixed layer depth: a subsurface proxy of ocean-atmosphere variability, J. Geophys. Res., 111, C07010, doi:10.1029/2003JC002157, 2006.

Roemmich, D., Riser, S., Davis, R., and Desaubies, Y.: Autonomous profiling floats: workhorse for broad-scale ocean observations, Mar. Technol. Soc. J., 38, 21–29, 2004.

Ruddick, B.: A practical indicator of the stability of the water column to double-diffusive activity,

OSD

7, 1469–1495, 2010

T/S compensation on upper ocean structure

R. W. Helber et al.

Deep-Sea Res., 30, 1105–1107, 1983.
Rudnick, D. L. and Martin, J. P.: On the horizontal density ratio in the upper ocean, Dynam. Atmos. Oceans, 36, 3–21, 2002.
Teague, W. J., Carron, M. J., and Hogan, P. J.: A comparison between the Generalized Digital Environmental Model and Levitus Climatologies, J. Geophys. Res., 95, 7167–7183, 1990.
Turner, J. S.: Buoyancy Effects in Fluids, Cambridge University Press, Cambridge, MA/USA, 367 pp., 1973.
Tippins, D. and Tomczak, M.: Meridional Turner angles and density compensation in the upper ocean, Ocean Dynam., 53, 332–342, 2003.
Wilks, D. S.: Statistical Methods in the Atmospheric Sciences, 2nd ed., Academic Press as an imprint of Elsevier, Boston, 627 pp., 2006.
Wong, A. P. S. and Johnson, G. C.: South Pacific eastern subtropical mode water, J. Phys. Oceanogr., 33, 1493–1509, 2003.
Yeager, S. G. and Large, W. G.: Observational evidence of winter spice injection, J. Phys. Oceanogr., 37, 2895–2919, 2007.
You, Y.: A global ocean climatological atlas of Turner angle: implications for double-diffusion and water-mass structure, Deep-Sea Res. Pt. I, 49, 2075–2093, 2002.

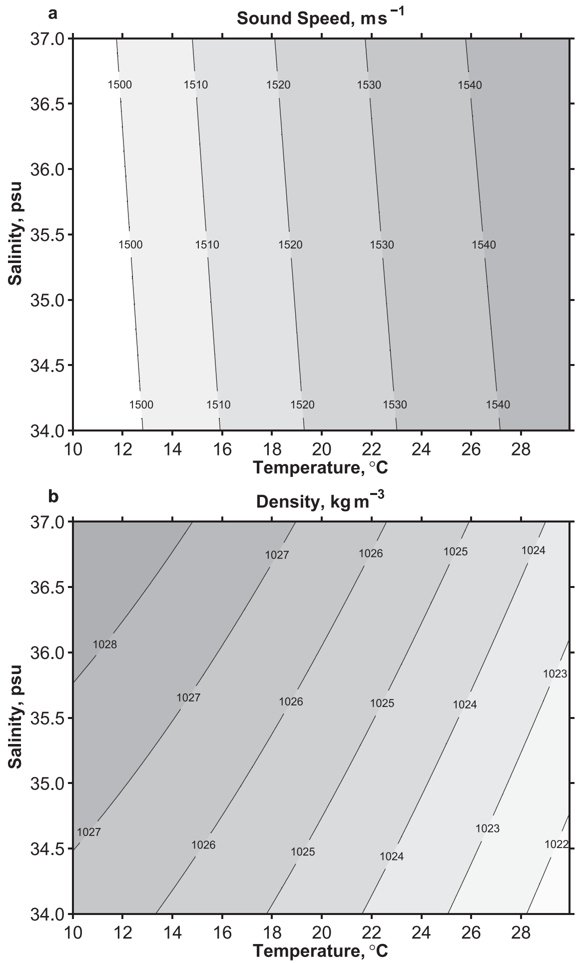

Fig. 1. Contours of sea water **(a)** sound speed in $\mathrm{m\,s^{-1}}$ and **(b)** density in $\mathrm{kg\,m^{-1}}$ as they vary with salinity and temperature.

OSD
7, 1469–1495, 2010

T/S compensation on upper ocean structure

R. W. Helber et al.

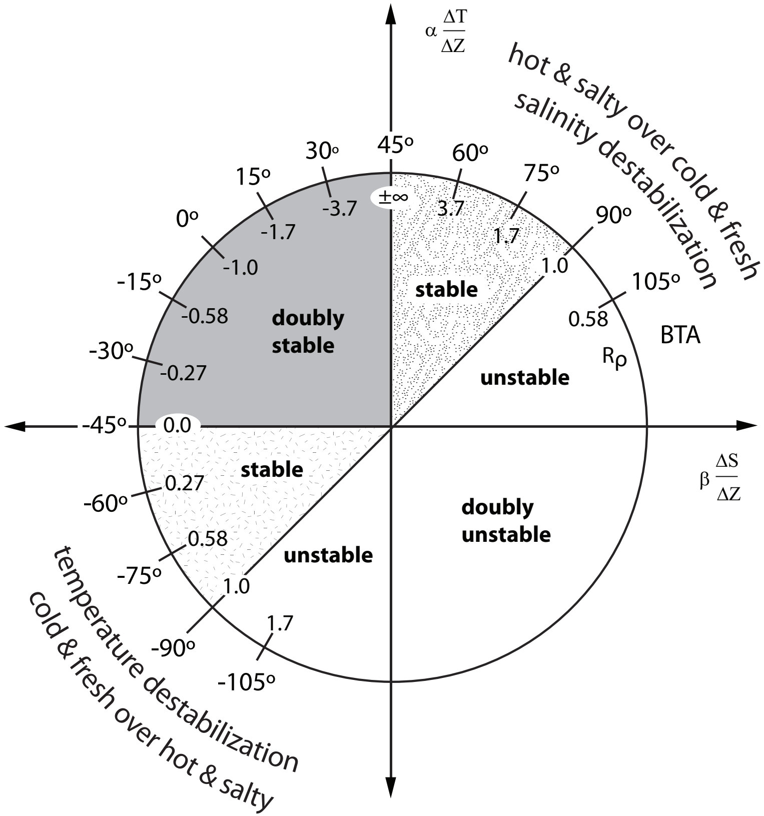

Fig. 2. A schematic diagram for the values of bulk Turner angle, BTA, and density ratio, R_ρ, with the change in density due to temperature on the y-axis and the change in density due to salinity on the x-axis. Quadrants are labeled for the total water column stability inside the circle with the T versus S contribution to stability and vertical compensating (or spicy) T and S changes outside the circle. The upper-left and lower-right quadrants correspond to doubly stable and unstable non-compensating T and S changes, respectively.

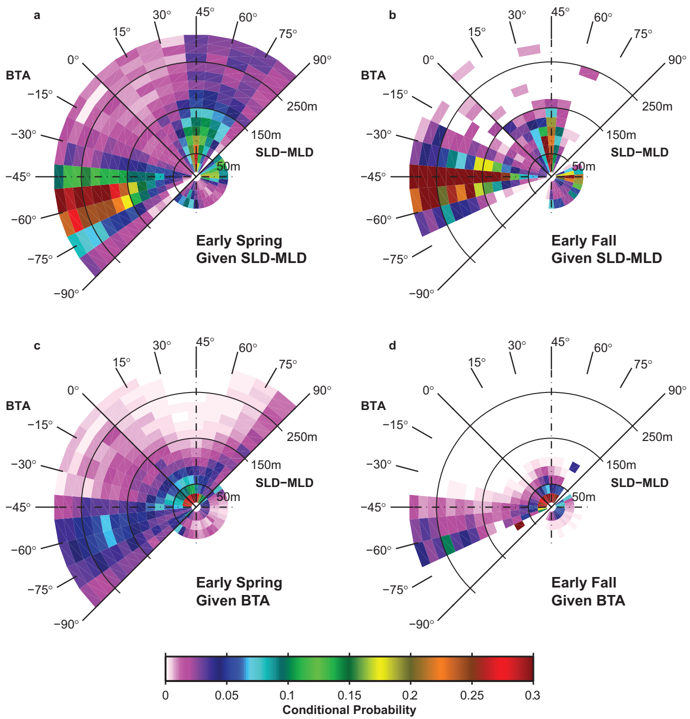

Fig. 3. Polar diagrams of conditional probability of BTA (in 10° bins) given SLD-MLD (in 20 m bins) for **(a)** early-spring (boreal January–March and austral July–September) and **(b)** early-fall (boreal July–September and austral January–March). Conversely, he conditional probability for SLD-MLD given BTA is shown in **(c)** for early-spring and **(d)** for early-fall (bins and months are the same as in **(a)** and **(b)**). The radial axis is the value of SLD-MLD with negative values plotted in the lower right. The angels are values of BTA. The conditional probabilities in **(a)** and **(b)** sum to one along the arcs for a given SLD-MLD bin while in **(c)** and **(d)** the radials for a given BTA bin sum to one.

OSD
7, 1469–1495, 2010

T/S compensation on upper ocean structure

R. W. Helber et al.

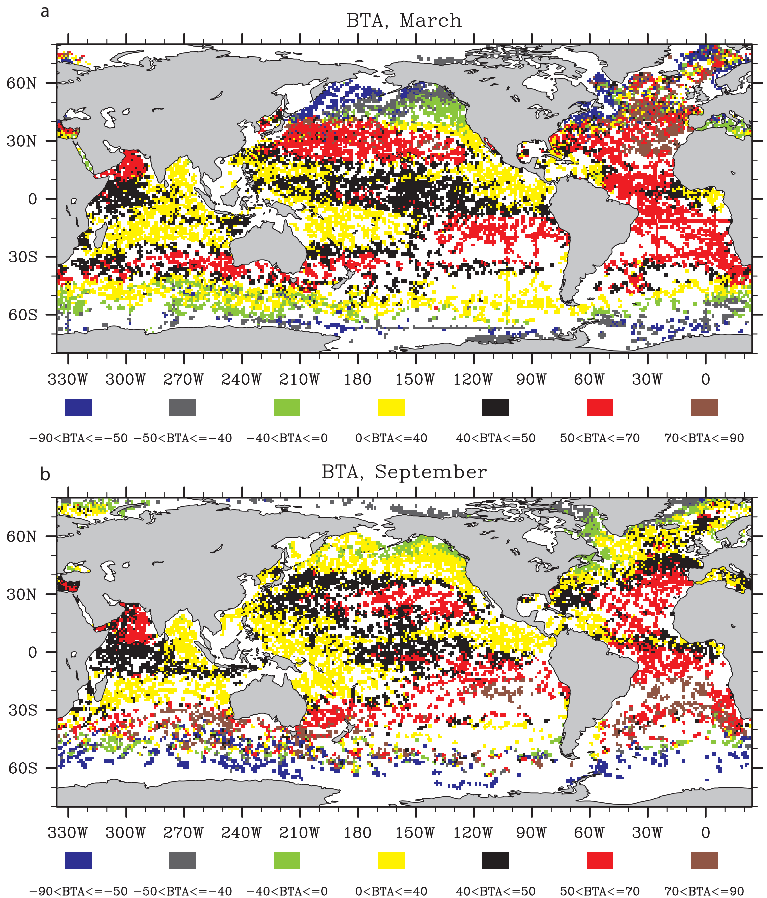

Fig. 4. The bulk Turner angle (BTA) globally for the month of **(a)** March and **(b)** September. Each square represents the median BTA value in a range specified by the color codes for all available data within a 1° radius circle.

OSD
7, 1469–1495, 2010
T/S compensation on upper ocean structure
R. W. Helber et al.

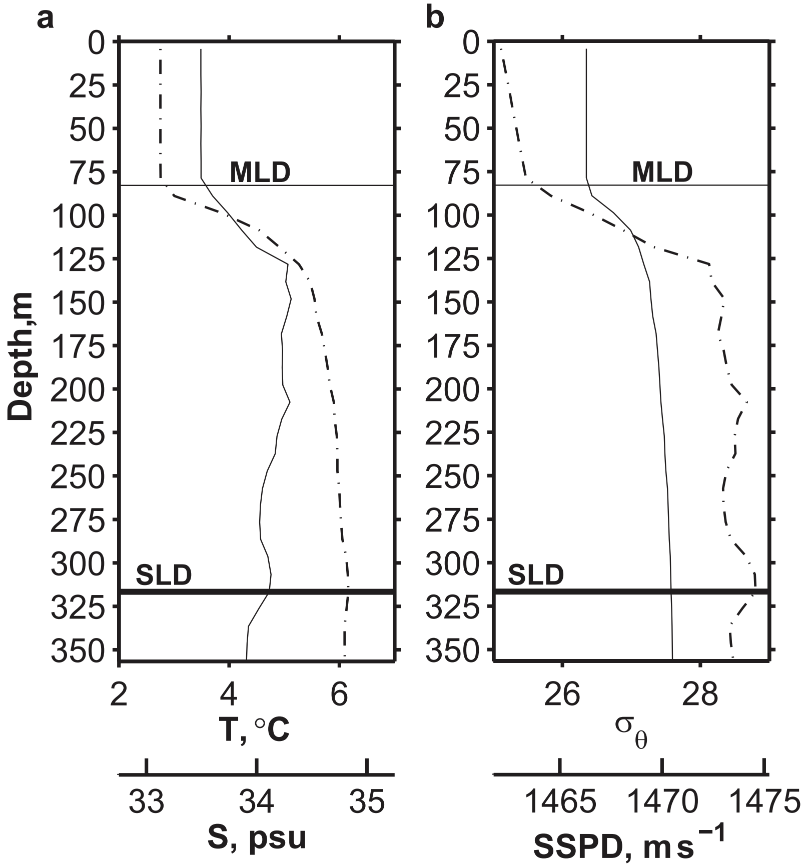

Fig. 5. An example profile of **(a)** temperature (solid) and salinity (dash-dot) and **(b)** sigma-theta (solid) and sound speed (dash-dot) in the temperature destabilizing regime (BTA=−53°) with a large difference between MLD (83 m) and SLD (317 m). The profile was made during February near the New Foundland Grand Banks (43.5° N, 56.0° W).

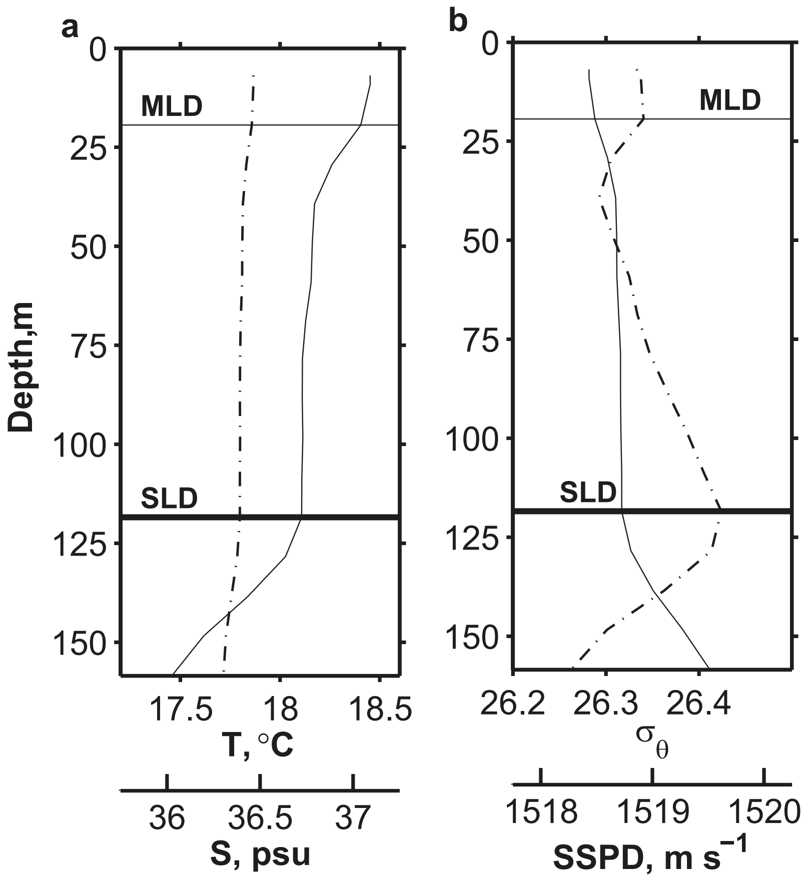

Fig. 6. An example profile of **(a)** temperature (solid) and salinity (dash-dot) and **(b)** sigma-theta (solid) and sound speed (dash-dot) in the salinity destabilizing regime (BTA=67°) and with a large difference between MLD (19 m) and SLD (118 m). The profile was made during February in the middle of the North Atlantic gyre (33.6° N, 33.9° W).

OSD
7, 1469–1495, 2010

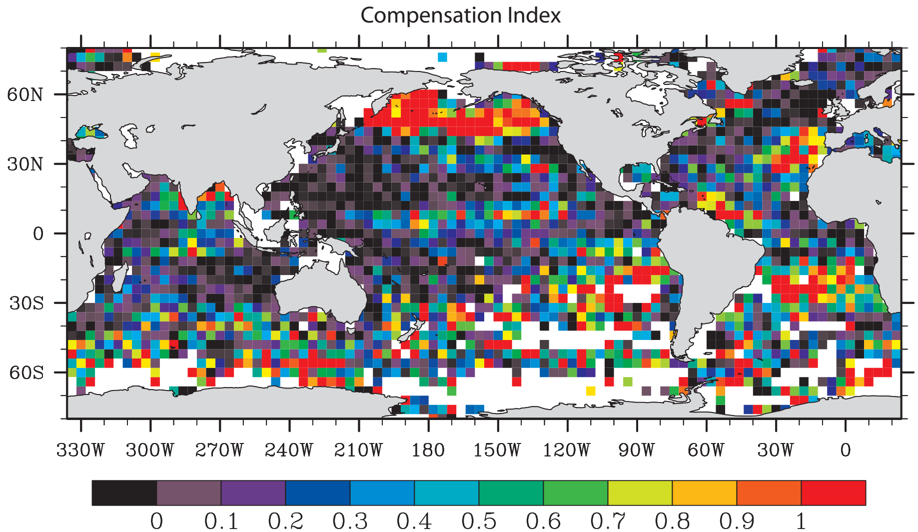

Fig. 7. The geographical map of the compensation index constructed using regressions for MLD for all available observations. Compensation index of 1 represents 4° by 4° regions where BTA is the sole predictor of MLD and 0 for regions where ILD is the sole predictor of MLD.

OSD
7, 1469–1495, 2010